

PHOTOMASK

BACUS—The international technical group of SPIE dedicated to the advancement of photomask technology.

BACUS

N • E • W • S

NOVEMBER 2019
VOLUME 35, ISSUE 11

PUV18 - 3rd Zeiss Student Poster

Using 3D Monte Carlo Simulation to Develop Resists for Next-Generation Lithography

Hayden R. Alty, Scott M. Lewis, Stephen G. Yeates, and Richard E. P. Winpenny, School of Chemistry, The University of Manchester, Oxford Road, Manchester M13 9PL, United Kingdom

ABSTRACT

This paper investigates the ability of a novel and bespoke Monte Carlo simulation to model the experimental outcome of exposure of resist materials by electron beam. The resists are a family of organo-metallic Chromium rings ($\text{Cr}_8\text{F}_8(\text{O}_2\text{CtBu})_{16}$), which have high resolution and low LER making them ideal candidates for the fabrication of the next generation of photomasks for EUV lithography. The model shows how the electron scattering in the resist material and the subsequent production of secondary electrons lead to the resists high resolution. The resist family can be modified to increase speed by up 17.3 times, by replacing the pivalate ligand with a methacrylate ligand, whilst still maintaining their desirable properties.

1. Introduction

All modern consumer electrical good contain microprocessors and most simple tasks are becoming dependent on this technology. The success of the microprocessor and the semiconductor industry is due to the constant progress of increasing processing power and miniaturization. This progress is driven by 'Moore's law' which is an observation made by Gordon Moore in 1965, that the number of integrated circuits per unit

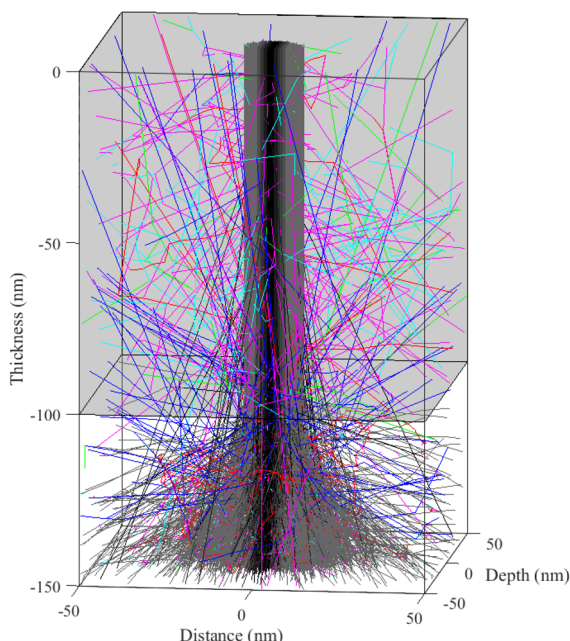


Figure 1. An Example plot of a 3D simulated image of electron tracks. Primary electrons are plotted in greyscale, backscattered electrons are blue, fast secondary electrons are red, slow secondary electrons are magenta, 2nd generation slow electrons are cyan and 3rd Generation slow electrons are green.

Please share with graduate students:

The \$10,000 **2020 Nick Cobb Scholarship** supports the education of a graduate student studying in a field related to advanced lithography.

Applications are due
1 November 2019.

For more information:
spie.org/nickcobb

**TAKE A LOOK
INSIDE:**

INDUSTRY BRIEFS
—see page 8

CALENDAR
For a list of meetings
—see page 9

SPIE.

EDITORIAL

Juxtaposition

Larry Zurbrick, Keysight Technologies, Inc.

At the recent Photomask Technology / EUV conference in Monterey, we were brought up to date on the latest challenges, developments, progress, potential solutions and solutions encompassing EUV lithography and related mask making. The number and depth of expertise of all individuals and companies that are contributing to advancing the current and next generation EUV infrastructure is astounding. Rapid progress is being made as the cycles of learning accelerate. The insurmountable technical issues of the recent past are being addressed by bringing the best and brightest minds to bear of what were perceived as roadblocks to the technology. The first IC's are now being sold that have been produced with EUV lithography. But there is an interesting contrast to these leading-edge efforts.

The first presentation of the Photomask Technology conference following the plenary session was the 2019 Mask makers survey results. This is an annual "event" that I look forward to since it is a visible sign of the state-of-the state for those companies participating in the survey. Although a major focus of the concurrent conferences was on EUV technology, the majority of the almost 600,000 masks delivered since last year's survey were at nodes greater than or equal to 130 nm (~320,000 units per the data presented). Greater than 80% of the mask types delivered were Binary and a similar percentage were on chromium on glass substrates. Most (69%) of these masks are written on laser writers. EUV masks accounted for ~0.5% by type or substrate, less than 3,000 EUV masks! This presentation was followed by an invited talk from Franklin Kalk reviewing the challenges of sustaining the mask manufacturing base. The interesting point of all of this is that the majority of masks being produced today and probably in the future (when the IoT ramps) will be what we consider "trailing edge" technology written on laser writers. Franklin, in previous presentations, had pointed out the issues the industry is facing with dwindling support for legacy mask making equipment and the economics stacked against purchasing new "legacy" equipment to meet the future increased demand. One economic strategy that makes sense is to engineer and produce highly productive equipment for these "trailing edge" mask types. The other is to re-engineer legacy systems with updated technology to repair systems where components are no longer available. It sounds like an opportunity for a disruptive technology or business model to make an entrance into the market. Is anyone listening?



N • E • W • S

BACUS News is published monthly by SPIE for BACUS, the international technical group of SPIE dedicated to the advancement of photomask technology.

Managing Editor/Graphics Linda DeLano

SPIE Sales Representative, Exhibitions, and Sponsorships
Melissa Farlow

BACUS Technical Group Manager Marilyn Gorsuch

■ 2019 BACUS Steering Committee ■

President

Peter D. Buck, *Mentor Graphics Corp.*

Vice-President

Emily E. Gallagher, *imec*

Secretary

Kent Nakagawa, *Toppa Photomasks, Inc.*

Newsletter Editor

Artur Balasinski, *Cypress Semiconductor Corp.*

2019 Annual Photomask Conference Chairs

Jed Rankin, *GLOBALFOUNDRIES Inc.*

Moshe Preil, *KLA-Tencor Corp.*

International Chair

Uwe F. W. Behringer, *UBC Microelectronics*

Education Chair

Frank E. Abboud, *Intel Corp.*

Members at Large

Michael D. Archuletta, *RAVE LLC*

Brian Cha, *Samsung Electronics Co., Ltd.*

Derren Dunn, *IBM Corp.*

Thomas B. Faure, *GLOBALFOUNDRIES Inc.*

Aki Fujimura, *DS2, Inc.*

Brian J. Grenon, *Grenon Consulting*

Jon Haines, *Micron Technology Inc.*

Naoya Hayashi, *Dai Nippon Printing Co., Ltd.*

Bryan S. Kasproicz, *Photronics, Inc.*

Patrick M. Martin, *Applied Materials, Inc.*

Jan Hendrik Peters, *bmbg consult*

Stephen P. Renwick, *Nikon Research Corp. of America*

Douglas J. Resnick, *Canon Nanotechnologies, Inc.*

Thomas Scheruebl, *Carl Zeiss SMT GmbH*

Thomas Struck, *Infineon Technologies AG*

Bala Thumma, *Synopsys, Inc.*

Anthony Vacca, *Automated Visual Inspection*

Michael Watt, *Shin-Etsu MicroSi Inc.*

Larry Zurbrick, *Keysight Technologies, Inc.*

SPIE.

P.O. Box 10, Bellingham, WA 98227-0010 USA

Tel: +1 360 676 3290

Fax: +1 360 647 1445

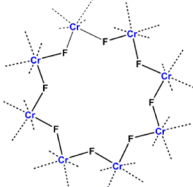
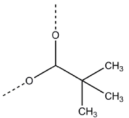
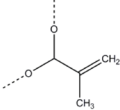
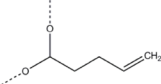
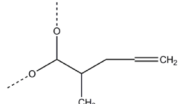
SPIE.org

help@spie.org

©2019

All rights reserved.

Table 1. A table of components of all the molecules simulated, including molecular formulas and diagrams.

Name	Formula	Diagram
Chromium Ring	Cr_8F_8	
Pivalate	$\text{O}_2\text{C}_5\text{H}_9$	
Methacrylate	$\text{O}_2\text{C}_4\text{H}_5$	
4-Pentenoate	$\text{O}_2\text{C}_5\text{H}_7$	
4-Methyl-4-Pentenoate	$\text{O}_2\text{C}_6\text{H}_9$	

area would double every year^[1]. Since Moore's observation the progress has slowed but has remained the benchmark and driving force for the semiconductor industry. The miniaturization of this technology is enabled by the ability to fabricate structures on the order of nanometres. These devices are fabricated using photolithography which uses a photomask to project a pattern onto a resist. In order to reach smaller feature sizes these photomasks require ever increasing resolution.

Electron Beam Lithography (EBL) is used in the production of around 30% of photomasks^[2] and is increasingly being used for mask repair. This increase in demand for masks with ever smaller feature sizes drives the need for improved EBL resists. These resists must meet the demand for smaller resolution (7nm node) and also reduce the write times for mask production. Developing such resists is a long, experimentally expensive, process of rapid prototyping to find suitable candidates followed by detailed characterisations to determine the resolution limits and development properties post exposure.

Currently, the majority of masks written using EBL are produced using Variable Shaped Beam (VSB) systems which use an acceleration voltage of 50kV, whereas other commercial lithography systems such as the Vistec EBPG5200, uses 100kV and the Raith E-line uses 30kV. This means that a resist that can be used at all commercial acceleration voltages and produce consistent results would be extremely beneficial.

1.1 Monte Carlo Simulation

Monte Carlo Modelling is a technique which uses pseudo random numbers as input into a probability distribution to find the average probability of an event. Monte Carlo techniques have long been used to simulate physical models and EBL is no exception with many already established methods of modelling electron scattering and interaction in a variety of materials. There are also several programs that provide useful data and interpretation for example CASINO, PENELOPE and Tracer. However, to fully understand exposure of resists by electron beam, not only do the initial (primary) electrons, from the incident beam, need to be considered but also secondary electrons which are generated in the resist. In many resist matrices these secondary electrons are the main mechanic for exposure. Compared to the incoming primary electrons they have much lower energy so scattering events, as well as inelastic collisions, are much

more likely and it is these events that break bonds creating free radicals, cross linking or chain scissioning. Therefore, secondary electrons are tracked up to 4th generation by this simulation. Electrons are tracked to their full extent within the bounds of the resist and the substrate, down to the energy of the weakest bond in the material. Below this any interactions will have too low an energy to cause any further exposure. Another important source of secondary electrons is Auger transitions as these generate electrons of desirable energies for exposure and will generate more secondary electrons as they travel through the resist.

1.2 Materials

The resists explored in this paper are all from the same family of modular resists being developed by the University of Manchester. They are negative tone organometallic resists that are comprised of a Chromium ring^[3] with an organic ligand attached around the ring. These organic ligands can be changed whilst the base chromium ring remains the same hence the modular nature. Here, the effect of changing these ligands in simulation will be explored in order to identify possible candidates for further investigation thus showing the potential of the model to reduce experimentation time.

Table 1 shows the components which make up the 4 molecules simulated in this paper. Each molecule consists of the Chromium ring with 16 ligands attached to the outside for example $\text{Cr}_8\text{F}_8(\text{Pivalate})_{16}$. These ligands change the solubility of the molecule which determines which casting solvents can be used.

2. Simulation

The Monte Carlo model consists of 4 major parts these being: 1. The "fast" scattering model is the foundation of the model and is used to track primary electrons and any electrons above 500eV; 2. A "slow" (low energy) quantum model which deals with low energy secondary electrons or any primary electrons if the resist and substrate are thick enough to prevent them escaping; 3. An Auger model which checks for generation of auger electrons; 4. A visualisation code used to generate different 3D plots of the electron tracks. For each section the main equations have been shown from each model, these being the collision probability and

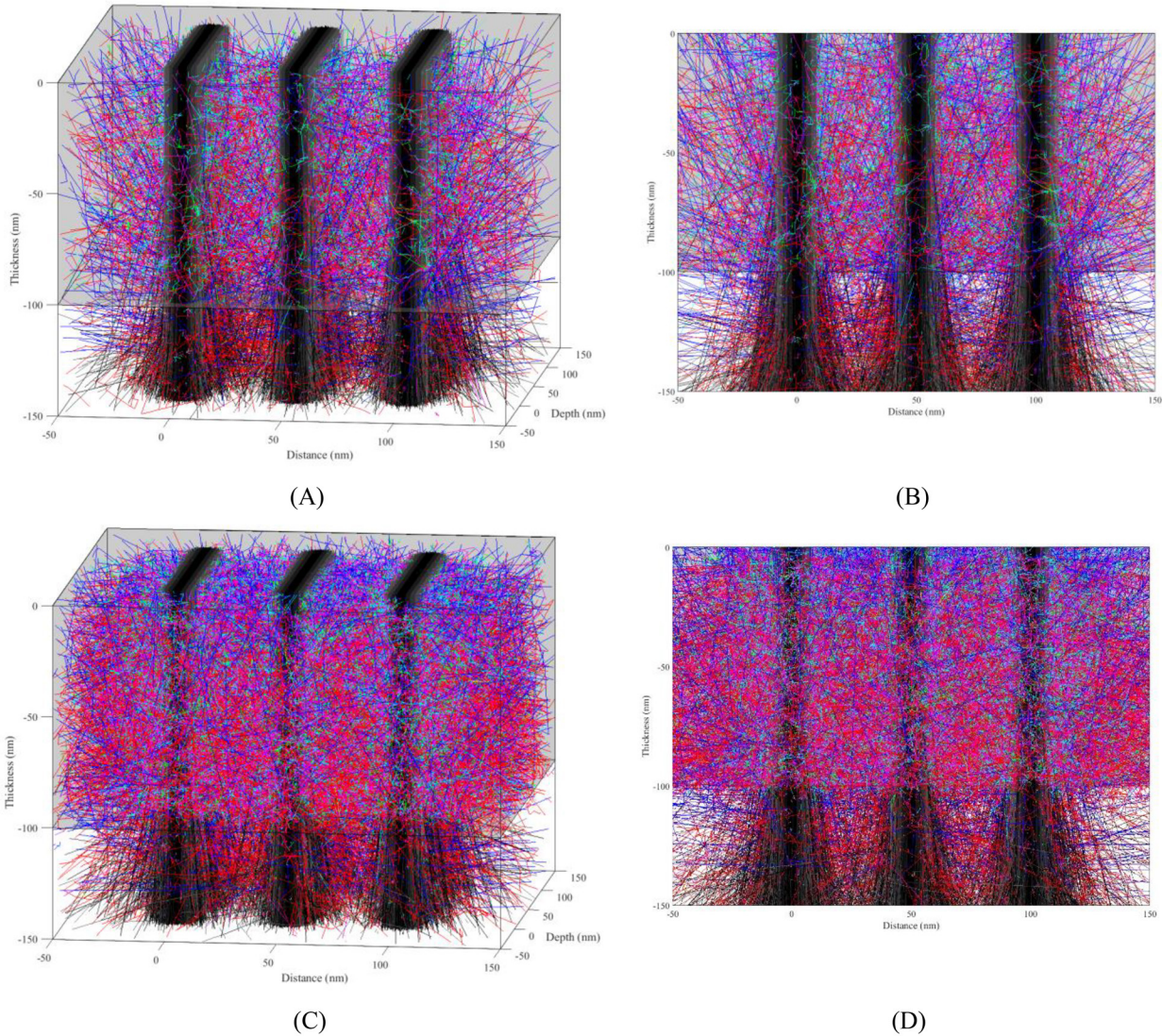


Figure 2. (A) A 3D plot of 100nm thick film of material **1** on a 50nm thick silicon substrate each line has a step size of 5nm and a pitch of 50nm. (B) A front on, cross section view of plot (A). (C) A 3D plot of 100nm thick film of material **2** on a 50nm thick silicon substrate each line has a step size of 5nm and a pitch of 50nm. (D) A front on, cross section view of plot (C). All images were produced with a beam energy of 50keV. Colours of different electrons are explained in figure 1.

energy loss of an electron in the material. There are further equations used to model the scattering angles and steps of the electron in order to build the full tracks and these are shown in a previous publication^[4].

2.1 Fast Scattering Model

The following model uses the model described by David C. Joy in *Monte Carlo Modelling for Electron Microscopy and Microanalysis*^[5] which is a classical model based on Rutherford scattering and as previously stated is only accurate for electrons with energy above 500eV.

As an electron travels through a material it will undergo both elastic and inelastic collisions. The cross section for inelastic collisions, $\sigma_{elastic}$ (cm²/atom), is given by,

$$\sigma_{elastic} = 5.21 \times 10^{-21} \frac{Z^2}{E^2} \frac{4\pi}{\alpha(1+\alpha)} \left(\frac{E+511}{E+1024} \right)^2 \quad (1)$$

where Z is the effective atomic number of the whole molecule and E is the energy of the incident electron (keV). The screening factor, α , is calculated using,

$$\alpha = 3.4 \times 10^{-3} \frac{Z^{0.67}}{E}. \quad (2)$$

The distance travelled by an electron between elastic collisions is the elastic mean free path, $\lambda_{elastic}$ (cm), and is given by,

$$\lambda_{elastic} = \frac{A}{N_a \rho \sigma_{elastic}} \quad (3)$$

where A is the molecular weight (g/mol), ρ is the density of the molecule (g/cm³) and N_a is Avogadro's constant. The inelastic scattering cross section is given by the following differential cross section,

$$\frac{d\sigma_{inelastic}}{d\Omega} = \frac{\pi e^4}{E^2} \left(\frac{1}{\Omega^2} + \frac{1}{(1+\Omega)^2} \right) \quad (4)$$

where E again is the energy of the incident electron and ΩE is the energy of the generated secondary electron. The mean free path for an inelastic scattering event is given by,

$$\lambda_{inelastic} = \frac{A}{N_a Z \rho \sigma_{inelastic}} \quad (5)$$

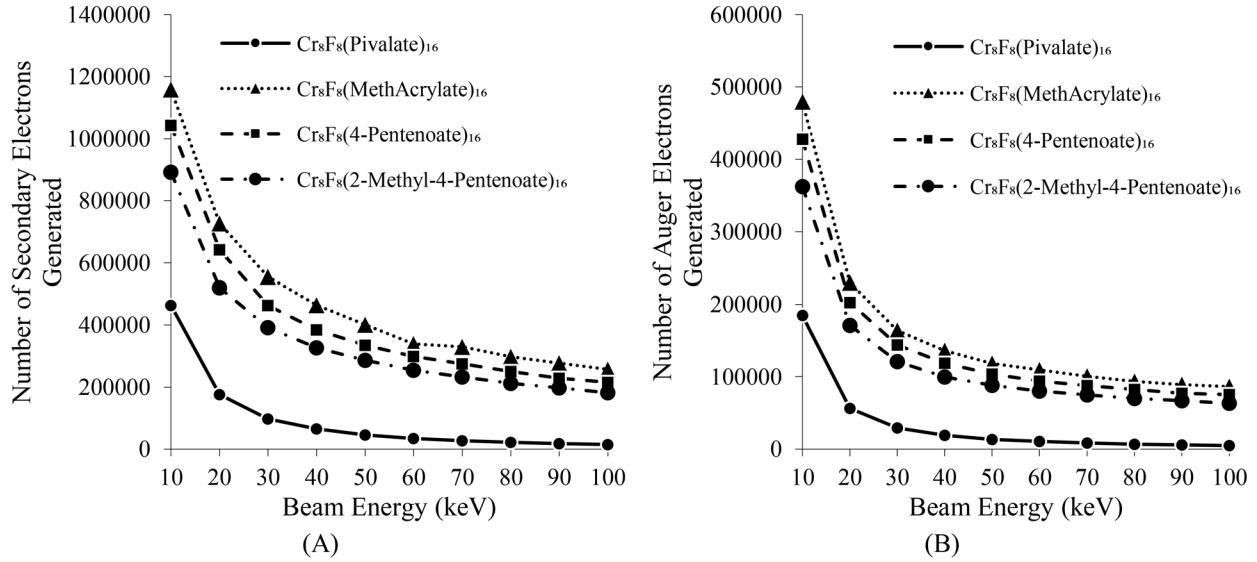


Figure 3. (A) A plot of secondary electrons generated in the 4 materials. Each material was simulated using 1 million electrons at acceleration voltages of 10-100kV. (B) A plot of auger electrons generated in the 4 materials. Each material was simulated using 1 million electrons at acceleration voltages of 10-100kV.

This simulation uses a constant energy loss model described by a modified Bethe-Bloch equation. The stopping power of a material, $\frac{dE}{ds}$ is given by,

$$\frac{dE}{ds} = 78500 \frac{Z}{AE} \ln \left(1.166 \frac{E + 0.86J}{J} \right) \quad (6)$$

where J is the min ionization potential (keV), calculated using,

$$J = \left[9.76Z + \frac{58.5}{Z^{0.15}} \right] \times 10^{-3} \quad (7)$$

2.2 Slow Scattering Model

In order to extend the model to account for lower energy (slow) electrons D Joy suggested a partial wave expansion method (PWEM). The PWEM used was described by J. J. Sakurai in *Modern Quantum Mechanics*^[6]. The slow scattering cross section is given by,

$$\sigma_{slow} = \frac{4\pi}{k^2} \sum_{l=0}^{\infty} (2l+1) \sin^2(ka)^{2l+1} \quad (8)$$

which when expanded for the dominant terms ($l=0,1,2,3$) gives,

$$\sigma_{slow} = \frac{4\pi}{k^2} (\sin^2(ka) + 3\sin^2(ka)^3 + 5\sin^2(ka)^5 + 7\sin^2(ka)^7) \quad (9)$$

where k is the wavenumber, $k = \frac{\sqrt{2ME}}{\hbar}$ and α was estimated to be $\sim 0.025\text{nm}$ (atomic radius of Carbon) \hbar using the Thomas-Fermi atomic radius approximation, $a = 0.468Z^{-\frac{1}{3}} \text{ \AA}$. The mean free path can be found using σ_{slow} in equation 3. Similarly, as with the fast scattering model the equations for generating scattering angels and steps between collisions has been omitted.

2.3 Auger Electrons

The inclusion of the production of secondary electrons through Auger transitions and cascades is important as the secondary electrons generated by these events are low energy. Therefore, they will create more secondary electrons as they travel through the material causing high amounts of local exposure. Auger electron emissions are more likely from transition to inner shells. This method was laid out by You et al^[7]. The cross section for inner shell ionizations is given by the Casnati cross section,

$$\sigma_c = \frac{a_0^2 F R^2 A B \ln U}{U E_U^2} \quad (10)^{[8]}$$

where a_0 is the first Bohr radius ($a_0 = 5.292 \times 10^{-11} \text{ m}$), R is the Rydberg energy ($R = 13.605 \text{ eV}$) and $U = E/E_U$, E is the energy of the incident electron and E_U is the binding energy of the shell. The other factors can be calculated by,

$$F = \left(\frac{2+J}{2+T} \right) \left(\frac{1+T}{1+J} \right)^2 \times \left[\frac{(J+T)(2+T)(1+J)^2}{T(2+T)(1+J)^2 + J(2+J)} \right]^{\frac{3}{2}} \quad (11)$$

$$A = \left(\frac{E_U}{R} \right)^d; B = 10.57 \exp \left(-\frac{1.736}{U} + \frac{0.317}{U^2} \right);$$

$$d = -0.0318 + \frac{0.3160}{U} - \frac{0.1135}{U^2};$$

$$J = \frac{E_U}{m_e c^2}; T = UJ$$

When Auger transitions occur, there can either be an electron or an X-ray emitted. The probability of an electron being emitted for the different transition channels is given by,

$$\gamma_{AX} = 1 - \frac{Z^4}{Z^4 + Z_0^4} \begin{cases} Z_0 = 32.4, & X = K \\ Z_0 = 89.4, & X = L \\ Z_0 = 155.9, & X = M \\ Z_0 = 300, & X = N \end{cases} \quad (12)^{[9]}$$

2.4 3D Visualisation

A separate code is used to plot the data in MATLAB. This is because matplotlib in Python, the language the simulation is written in, does not have a true 3D engine so the electron tracks do not plot correctly. Below is an example plot of a single beam entry point. In combination with the Monte Carlo simulation whole patterns of exposure can be plotted, depending on computational resources.

Figure 1. shows an example plot of a single spot of electron scattering. The resist (grey) thickness is 100nm on a silicon substrate with a thickness of 50 nm. The primary electrons are plotted in greyscale to show their distance from the centre point of the beam.

3. Results

Simulations were completed for the four materials: **1.** $\text{Cr}_8\text{F}_8(\text{Pivalate})_{16}$, **2.** $\text{Cr}_8\text{F}_8(\text{Methacrylate})_{16}$, **3.** $\text{Cr}_8\text{F}_8(4\text{-Pentenoate})_{16}$, **4.** $\text{Cr}_8\text{F}_8(2\text{-Methyl-4-Pentenoate})_{16}$. All materials were simulated as a 100nm thick layer on a 50nm thick substrate of Silicon. Material 1 is a known and tested material with a dose of $43,000 \mu\text{C}/\text{cm}^2$ at 100kV with a pitch of 60nm and is used as a comparison for the simulated values of the other materials. The properties for the materials used in the simulation are displayed in Table 2.

The properties of the materials shown in Table 2 give a good indication of how the materials will react in the simulation. From equation 1, for the

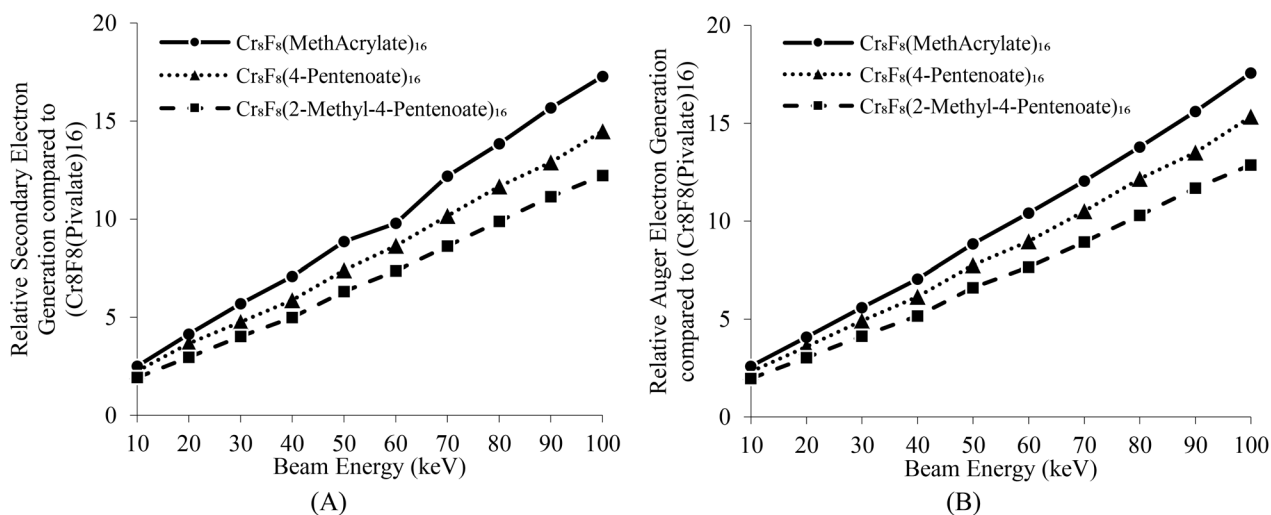


Figure 4. A plot of the ratio of Electrons generated in materials **2**, **3**, and **4** in comparison to material **1** for acceleration voltages 10-100kV.

elastic scattering cross section, it is clear that a higher Z value gives a larger scattering cross section which in combination with an increased stopping power (equation 6) means that the electrons will lose energy more quickly as they pass through the material. As an electron loses energy the probability of an inelastic scattering event increases as the mean free path for inelastic scattering events is inversely proportional to Z. This increase in inelastic scattering events means that more secondary electrons will be generated in the material. The generation of these secondary electrons cause chain scissioning and crosslinking in the material which leads to changes in solubility and hence exposure of the resist. The secondary electrons generated have a low energy compared to the primary electrons which means that they are much more likely to go on to generate more secondary electrons in a cascade. Similarly, with density, a higher density means a shorter mean free path between collisions meaning more scattering events will occur as an electron passes through the material. A low molecular weight also means a lower mean free path causing similar effects as those previously explained.

Knowing this, when comparing the resist materials, material **2** would be a much better candidate for increased electron sensitivity compared to the starting material **1**. This can clearly be seen in figure 2 where material **2** (C and D) has a large increase in secondary electrons generated in the resist when compared to material **1**.

Also, in these images the spread of the electron beam can be seen as it passes through the material, the broadening of the beam in the resist shows how the resolution will decrease. In both resist materials the beam remains unchanged showing that the high resolution of material **1** is maintained in material **2**. Both materials have the same number of incident primary electrons so that the increase in secondary electron generation can be seen. These are not real doses as material **2** would be over-exposed with this amount of electron generation.

The extent of the spread of secondary electrons can also be seen. This lateral exposure away from the line is responsible for the proximity effect and also a broadening of the structures. Due to the energy disparity between the high energy primary electron and much lower energy secondary electron, the generation angle of most first order secondary electrons is over 80°, which is the cause of the lateral direction. The green electrons in the plots are the lowest energy electrons and the highest generation of secondary electrons and they show where the highest level of exposure is occurring. This is where the most collisions are happening, hence the most electrons being generated and therefore where the resist is being exposed. These materials have a high resolution due to the low amount of lateral exposure with these low energy secondary electrons being focused around the beam.

Even though there appears to be more electrons generated in the resist compared to the silicon substrate this is not the case. It is due to

the mean free path being so much lower in the silicon. This means that the electrons cannot travel as far before their energy is lost, so they are contained within the center of the beam and so are obscured in the image by the divergence of the beam. The high scattering properties of silicon also mean that large amounts of resist exposure occur at the resist-silicon interface, due to backscattering of low energy electrons from the silicon into the resist.

Figure 3 shows the number of secondary electrons and the number of auger electrons generated in all four materials for beam energies in the range of 10 to 100keV. This range was chosen as it covers most conventional lithography energies, with the resist family in this paper usually being written at 30 and 100 kV and with the common industry technique VSB being at 50kV. 1,000,000 incident electrons were used in the simulations of all the materials at all energies, as this provides a sufficiently large data size to reduce statistical error. It is clear to see that as the energy increases the number of secondary electrons generated also decreases. This is due to the scattering cross sections being inversely proportional to the energy of the incident electron. So, as the energy increases, the chance of collisions and hence generation of secondary electrons decreases. This also means that while the resist is less sensitive at higher energies it will also have better resolution. These results confirm those shown in figure 2 where material **2** is the most sensitive of the four materials. While it may seem that the number of inner shell ionizations would decrease with lower energy this is only apparent for the K shell. The L, M and N shell transitions start to dominate at lower electron energies meaning that auger electrons become a large contributor to the exposure of the resist as long as the incident beam energy is kept above the highest electron binding energy of the molecule.

Figure 4 shows the relative number of secondary electrons generated in each material when compared to material **1**. This shows an increase in electron generation for each material (**2,3&4**) when compared to a known and tested material (i.e. material **1**). From table 2 it is clear why material **2** and **3** should be faster as they have properties which are more conducive of electron scattering. However, material **4** does not have these properties yet still has an increase by a factor of 12.8. This increase is because the ligands that replace the pivalate on the chromium ring have an exposed double carbon bond on the end of the molecule. This means that when secondary electrons are generated from the molecule there is a high chance that two electrons are emitted causing a large increase in electron generation when an electron collides with the ligand. Also, the reduction of carbon and hydrogen in the molecules increases the effective Z and the density of the molecule leading to reduced mean free path and consequently more collisions. This data shows that the molecules presented here would offer an increase in generation of secondary electrons and hence an increase of sensitivity of 17.3 times for material **2** at 100kV.

4. Conclusion

New generations of a family of resists were explored using Monte Carlo Modelling. New potential candidates for improvement to the resist material have been found by simulating a change in ligand on the metallic ring. A potential improvement in dose by a factor of 17.3 was found by replacing the pivalate ligand on the current material with a methacrylate ligand. This estimation of the increase in dose does not take into account many factors which affect the dose of a resist material such as solubility in the casting and developing solvents. Changing these ligands will greatly change their solubility. Also due to this change in solubility the LER and resolution of the material will be affected beyond what is suggested by the simulations. Overall this shows that costly and time-consuming experimentation can be reduced by using simulation before chemical synthesis and testing of the resist material is required.

5. References

- [1] G. E. Moore, "Cramming more components onto integrated circuits", *Electronics*, Volume 38, Number 8, April 19, (1965).
- [2] Fujimura, A., Willis, A., "2017 mask maker survey conducted by the eBeam Initiative", *Proc. SPIE*, **10451** (2017).
- [3] Lewis, S. M., Fernandez, A., DeRose, G. A., Hunt, M. S., Whitehead, G. F. S., Lagzda, A., Alty, H. R., Ferrando-Soria, J., Varey, S., Kostopoulos, A. K., Schedin, F., Murn, C. A., Timco, G. A., Scherer, A., Yeates, S. G., and Winpenny, R. E. P., "Use of Supramolecular Assemblies as Lithographic Resists", *Supplementary Information*, *Angew. Chem. Int. Ed.*, **56**, (24), 6749-6752 (2017).
- [4] Laye, R. H., Larsen, F. K., Overgaard, J., Murn, C. A., McInnes, E. J. L., Rentschler, E., Sanchez, V., Teat, S. J., Güdel, H. U., Waldmann, O., Timco, G. A., and Winpenny, R. E. P., "A family of heterometallic wheels containing potentially fourteen hundred siblings", *Chem. Commun.*, **9**, 1125-1127 (2005).
- [5] Joy, D. C., "Monte Carlo Modeling for Electron Microscopy and Microanalysis", New York: Oxford University Press, (1995).
- [6] Sakurai, J. J., and Tuan, San Fu., "Modern Quantum Mechanics.", Menlo Park, California; Wokingham: Benjamin-Cummings, (1985).
- [7] You, D. S., Li, H. M., and Ding, Z. J., "Monte Carlo simulation of Auger electron emission from thin film on substrate" *J. Electron Spectrosc. Relat. Phenom.*, **222**, 156-161 (2018).
- [8] Casnati, E., Tartari, A., and Baraldi, C., "An empirical approach to K-shell ionisation cross section by electrons", *J. Phys. B: At. Mol. Phys.* **15** 155 (1982).
- [9] Matthew, J.A.D., "The Auger Process, Scanning Auger Electron Microscopy", John Wiley & Sons, Ltd, pp. 15-44 (2007)

Table 2. A table of values of all the molecules simulated including effective atomic number, Z; Molecular weight, A and Density, ρ . *Density values for Materials 2, 3 and 4 are estimated from the measured value for 1 and the change in ligand density.

Name	Formula	Effective Atomic Number, Z	Molecular Weight, A, (g/mol)	Density*, ρ , (g/cm ³)
1. Cr ₈ F ₈ (Pivalate) ₁₆	Cr ₈ F ₈ O ₃₂ C ₈₀ H ₁₄₄	8.93	2192	1.21
2. Cr ₈ F ₈ (Methacrylate) ₁₆	Cr ₈ F ₈ O ₃₂ C ₆₄ H ₈₀	9.85	1929	1.32
3. Cr ₈ F ₈ (4-Pentenoate) ₁₆	Cr ₈ F ₈ O ₃₂ C ₈₀ H ₁₁₂	9.26	2154	1.28
4. Cr ₈ F ₈ (4-Methyl-4-Pentenoate) ₁₆	Cr ₈ F ₈ O ₃₂ C ₉₆ H ₁₄₄	8.79	2378	1.25
Silicon	Si	14	28.09	2.3



N • E • W • S

Sponsorship Opportunities

Sign up now for the best sponsorship opportunities

Photomask Technology + EUV Lithography 2020

Contact: Melissa Farlow,
Tel: +1 360 685 5596; melissaf@spie.org

Advanced Lithography 2020

Contact: Teresa Roles-Meir,
Tel: +1 360 685 5445; teresar@spie.org

Advertise in the BACUS News!

The BACUS Newsletter is the premier publication serving the photomask industry. For information on how to advertise, contact:

Melissa Farlow,
Tel: +1 360 685 5596
melissaf@spie.org

BACUS Corporate Members

Acuphase Inc.
American Coating Technologies LLC
AMETEK Precitech, Inc.
Berliner Glas KGaA Herbert Kubatz GmbH & Co.
FUJIFILM Electronic Materials U.S.A., Inc.
Gudeng Precision Industrial Co., Ltd.
Halocarbon Products
HamaTech APE GmbH & Co. KG
Hitachi High Technologies America, Inc.
JEOL USA Inc.
Mentor Graphics Corp.
Molecular Imprints, Inc.
Panavision Federal Systems, LLC
Profilcolore Srl
Raytheon ELCAN Optical Technologies
XYALIS

Industry Briefs

■ TSMC's Leading-Edge Fab Investments Set Stage for Sale Surge in 2H19

Taiwan Semiconductor Manufacturing Company's investments in advanced wafer-fab technology are set to pay off for the world's largest foundry as it continues the production ramp of 7nm ICs. TSMC is expected to have over 7x the dollar volume sales at <40nm processes as compared to the combined 2019 total of GlobalFoundries, UMC, and SMIC (\$22.9 billion versus \$3.2 billion). SMIC entered initial production of 28nm technology more than three years after TSMC began fabricating wafers with its 28nm process. SMIC expects recognizable revenue from its new 14nm FinFET technology in the fourth quarter of this year (and introduce 12nm FinFET technology in 2020), once again three years behind TSMC's introduction of similar processes.

The pace at which TSMC's customers adopt leading-edge technologies has quickened, as well. It took eight quarters for the foundry's 40-45nm technology to secure greater than 20% of its total sales, five quarters for its 28nm process to exceed that threshold, and only three quarters for its 7nm process to account for more than 20% of its quarterly revenue. Amazingly, the company believes that its ramp of 5nm technology, as a percent of its sales, will be even faster than its 7nm process!

<https://www.semiconductor-digest.com/2019/10/09/tsmcs-leading-edge-fab-investments-set-stage-for-sale-surge-in-2h19/>

■ ASML tops profit forecast and sees surge in bookings

Semiconductor equipment maker ASML beat quarterly profit and bookings forecasts on Wednesday, continuing a strong run of results for its latest chipmaking equipment. The Dutch firm's shares have surged 75% this year, shrugging off weak end-markets for semiconductor producers as ASML's cutting-edge equipment remains in demand from computer chip heavyweights like Samsung and Taiwan Semiconductor. Third-quarter profit came in at \$692 million, beating analysts' average forecast of 609 million, though down on the 680 million made in the same period last year. ASML shares dipped 1.0 percent after closing at an all-time high of 243.2 euros. The stock's rise has seen the company's equity market value top 100 billion euros. Third-quarter sales of 3 billion euros were driven by demand for 5G telecom network and artificial intelligence applications.

<https://www.reuters.com/article/us-asml-results/asml-tops-profit-forecast-and-sees-surge-in-bookings-idUSKBN1WV0FW>

■ China semiconductor revenues increase 11.8% in 1H19, says Digitimes Research

Eric Chen, DIGITIMES Research, Taipei, Thursday 26 September 2019

Despite the global semiconductor industry's weakening, China's semiconductor industry continued to perform stably with sales rising 11.8% year on year. It is likely to continue being constrained by the economy, US-China trade tensions and a lack of advanced technology and talent. However, for the medium to long term, demand created by emerging technologies and support from government are expected to drive China's semiconductor growth.

Of the global sales in the first half, over 30% were contributed by China, the largest semiconductor market. Cities in the eastern coast of China are still the hub of the country's semiconductor industry, but several western cities including Xian, Chengdu and Wuhan, have also been aggressively developing applications to become another hub.

Despite the effort of the China government, the local semiconductor industry still cannot function independently much. Currently, China-based players can supply less than 5% of ICs for high-end and specific applications, and the problem is becoming more critical because of the trade war between China and the US. In the IC design sector, China has been accelerating local capability in the entry-level to mid-range segments, but it still depends heavily on US-based ICs in the high-end segment. As for raw materials and equipment, Chinese suppliers only have a very small presence and the industry is highly dependent on the US and Japan for supply.

<https://www.digitimes.com/news/a20190926PD204.html>

Join the premier professional organization for mask makers and mask users!

About the BACUS Group

Founded in 1980 by a group of chrome blank users wanting a single voice to interact with suppliers, BACUS has grown to become the largest and most widely known forum for the exchange of technical information of interest to photomask and reticle makers. BACUS joined SPIE in January of 1991 to expand the exchange of information with mask makers around the world.

The group sponsors an informative monthly meeting and newsletter, BACUS News. The BACUS annual Photomask Technology Symposium covers photomask technology, photomask processes, lithography, materials and resists, phase shift masks, inspection and repair, metrology, and quality and manufacturing management.

Individual Membership Benefits include:

- Subscription to BACUS News (monthly)
- Eligibility to hold office on BACUS Steering Committee

spie.org/bacushome

Corporate Membership Benefits include:

- 3-10 Voting Members in the SPIE General Membership, depending on tier level
- Subscription to BACUS News (monthly)
- One online SPIE Journal Subscription
- Listed as a Corporate Member in the BACUS Monthly Newsletter

spie.org/bacushome

C A L E N D A R

2020



SPIE Advanced Lithography

23-27 February 2020
San Jose Marriott and
San Jose Convention Center
San Jose, California, USA



Photomask Japan

19-20 April 2020
Yokohama, Japan



The 36th European Mask and Lithography Conference, EMLC 2020

22-24 June 2020
Leuven, Belgium



SPIE Photomask Technology + EUV Lithography

20-24 September 2020
Monterey Conference Center and
Monterey Marriott
Monterey, California, USA

SPIE is the international society for optics and photonics, an educational not-for-profit organization founded in 1955 to advance light-based science, engineering, and technology. The Society serves nearly 264,000 constituents from 166 countries, offering conferences and their published proceedings, continuing education, books, journals, and the SPIE Digital Library in support of interdisciplinary information exchange, professional networking, and patent precedent. SPIE provided more than \$4 million in support of education and outreach programs in 2018. spie.org

SPIE.

International Headquarters
P.O. Box 10, Bellingham, WA 98227-0010 USA
Tel: +1 360 676 3290
Fax: +1 360 647 1445
help@spie.org • spie.org

Shipping Address
1000 20th St., Bellingham, WA 98225-6705 USA

Managed by SPIE Europe

2 Alexandra Gate, Ffordd Pengam, Cardiff,
CF24 2SA, UK
Tel: +44 29 2089 4747
Fax: +44 29 2089 4750
spieeurope@spieeurope.org • spieeurope.org

You are invited to submit events of interest for this calendar. Please send to lindad@spie.org.